SANDIA REPORT

SAND98–2683
Unlimited Release
Printed December 1998

Surface Micromachined Flexural Plate Wave Device Integrable on Silicon

B. A. Tuttle, J. A. Ruffner, W. R. Olson, W. K. Schubert, S. J. Martin, M. A. Mitchell, P. G. Clem, D. Dimos, and T. J. Garino

Prepared by
Sandia National Laboratories
Albuquerque, New Mexico 87185 and Livermore, California 94550

Sandia is a multiprogram laboratory operated by Sandia Corporation, a Lockheed Martin Company, for the United States Department of Energy under Contract DE-AC04-94AL85000.

Sandia National Laboratories

Issued by Sandia National Laboratories, operated for the United States Department of Energy by Sandia Corporation.

Available to DOE and DOE contractors from
Office of Scientific and Technical Information
P.O. Box 62
Oak Ridge, TN 37831

Prices available from (615) 576-8401, FTS 626-8401

Available to the public from
National Technical Information Service
U.S. Department of Commerce
5285 Port Royal Rd
Springfield, VA 22161

NTIS price codes
Printed copy: A03
Microfiche copy: A01

DISCLAIMER

Portions of this document may be illegible in electronic image products. Images are produced from the best available original document.

SAND98-2683
Unlimited Release
Printed December 1998

Surface Micromachined Flexural Plate Wave Device Integrable On Silicon

B.A. Tuttle, J. A. Ruffner and W.R. Olson
Electronic and Optical Materials Department

W.K. Schubert, S.J. Martin and M.A. Mitchell
Chemical Microsensors Department

P.G. Clem and D. Dimos
Direct Fabriction Technologies Department

T.J. Garino
Materials Processing Department
Sandia National Laboratories
P.O. Box 5800
Albuquerque, NM 87185-1405

Abstract

Small, reliable chemical sensors are needed for a wide range of applications, such as weapon state-of-health monitoring, nonproliferation activities, and manufacturing emission monitoring. Significant improvements in present surface acoustic wave sensors could be achieved by developing a flexural plate-wave (FPW) architecture, in which acoustic waves are excited in a thin sensor membrane. Further enhancement of device performance could be realized by integrating a piezoelectric thin film on top of the membrane. These new FPW-piezoelectric thin film devices would improve sensitivity, reduce size, enhance ruggedness and reduce the operating frequency so that the FPW devices would be compatible with standard digital microelectronics. Development of these piezoelectric thin film // FPW devices requires integration of (1) acoustic sensor technology, (2) silicon micromachining techniques to fabricate thin membranes, and (3) piezoelectric thin films. Two piezoelectric thin film technologies were emphasized in this study: $Pb(Zr,Ti)O_3$ (PZT) and AlN. PZT thin films were of sufficient quality such that the first high frequency SAW measurements on PZT thin films were measured during the course of this study. Further, reasonable ferroelectric properties were obtained from PZT films deposited on Si surface micromachined FPW device membranes. Fundamental understanding of the effect of nanodimension interfacial layers on AlN thin film domain configurations and piezoelectric response was developed.
Sandia is a multiprogram laboratory operated by Sandia Corporation, a Lockheed Martin Company, for the US Department of Energy under contract DE-ACO4-94AL85000.

Acknowledgments

The authors acknowledge enlightening technical discussions and program direction from Gordon Pike and Jamie Wiczer. The efforts of Steve Chang, Jim Smith and William Eaton in the development of the Si surface micromachined devices and technical information concerning micromachining technology is gratefully acknowledged. Gary Zender, Bonnie Mckenzie and Mike Eatough provided excellent materials analysis support. Steve Lockwood and Amelia Sanchez made substantial contributions to this program with their PZT thin film solution synthesis and PZT film deposition of some of the films used in this study.

Table of Contents

Figures

Tables

Introduction

This highly interdisciplinary project resulted in significant technical contributions in four technical areas:

(1) piezoelectric thin film development,
(2) development of process integration procedures for unit processes,
(2) device fabrication, and
(3) device characterization.

PZT thin films were fabricated by chemical solution deposition procedures, which are commonly, and often erroneously, termed sol-gel processing. Highly oriented AlN films were fabricated using reactive sputter deposition with piezoelectric coefficients that were in reasonable agreement with single crystal values. PZT thin films were chosen because of the large piezoelectric coefficients that are available in this material system, 200 times greater than that of quartz. AlN films were chosen for investigation, since they have piezoelectric coefficients approximately 20 times greater than quartz and loss that is substantially less than that for PZT. An array of devices were fabricated during the course of this program including PZT//FPW devices using both surface and bulk Si micromachining, surface acoustic wave (SAW) devices on both conducting and nonconducting substrates, PZT thin film // bulk silicon micromachined microcantilever beams and piezoelectric thin film // Si macrocantilever beams.

Piezoelectric Thin Film Development

AlN Films

Deposition parameters were found to have a marked effect on piezoelectric response of reactively sputtered AlN thin films. We observed piezoelectric response values ranging from -3.5 to + 4.2 pm/V for 1-2 μm thick AlN films deposited onto Ti//Ru electrode stacks. An investigation of the effects of deposition parameters, in particular the nature of the interfaces between subsequently deposited layers in the Ti//Ru//AlN stack structure, was conducted. The lag time between deposition of adjacent thin film layers or between presputtering (cleaning) and actual deposition from the sputtering targets seemed to have the greatest affect on the sign of the piezoelectric response. This suggests that chemical reaction occurring either on the target or the pristine thin film surface may be responsible for changing an important thin film property such as domain orientation within the AlN.

AlN is an excellent material for use in flexural plate wave devices used for sensing devices for a variety of reasons. First it offers good piezoelectric response, with a piezoelectric coefficient of 5.4 pm/V, coupling coefficient of 0.1 and Q factor of 5,000 at 10 MHz. AlN also offers excellent flexural strength (5,000 kg/cm^3), high electrical resistivity ($10^{11} - 10^{14}$ Ω cm), low thermal expansion (4.5 ppm/°C) and low toxicity. Although its piezoelectric properties are well known, the growth mechanisms of reactively sputter deposited AlN thin films are not well understood. In particular, the effect of deposition parameters on the resultant thin film crystalline, microstructural, and dipole orientation properties are of considerable importance for achieving optimal piezoelectric response reproducibly.

Early in this research, it was discovered that many of our sputtered AlN samples exhibited near zero piezoelectric responses, while some exhibited positive values and others exhibited negative values. A change in magnitude might be indicative of a difference in crystalline orientation, grain size, or concentration of defects. However, a change in sign of piezoelectric response indicates not a change in film quality, but a complete reversal of some property. The likely property in the case of the AlN thin films is the net dipole orientation. A change in the net dipole orientation could explain a number of phenomena that we observed in our early experiments including that piezoelectric response (1) could exhibit a positive, negative, or zero value, (2) could vary markedly for AlN thin films exhibiting the same crystallographic orientation per x-ray diffraction results, and (3) could be strongly dependent on conditions at the thin film interfaces and subsequently the entire thin film deposition process. Previous researchers have performed etching experiments on $LiNbO_3$ crystals and determined that etch rate was highly dependent upon dipole orientation.

Experimental Procedures for AlN Films

Several multilayered samples were sputter deposited and tested in order to determine the effect of presputter target conditioning on the resultant piezoelectric response. Silicon wafers with a 400 nm thick thermal oxide layer were used as substrates. Each substrate was sputter coated with 30 nm Ti, 100 nm Ru, and then 1 or 2 micron thick films of AlN that served as the adhesion, electrode, and piezoelectric layers respectively. All depositions were performed in a Unifilm PVD-300 Multisource Sputter Deposition Chamber (base pressure = 2×10^{-7} torr) using the deposition parameters listed in Table 1.

Table 1. Deposition parameters for Ti//Ru//AlN thin film samples.

	Ti	Ru	AlN
Thickness (nm)	20	100	1,000 or 2,000
Substrate temperature (°C)	300	300	500
Ar pressure (mTorr)	2.5	2.5	2
N2 pressure (mTorr)	0	0	0.2 – 0.5
Power	53 W DC	23 W DC	147 W RF
Deposition rate (nm/min)	7.9	5.9	7.9

The length of time between deposition of two sequential films was varied in order to determine the effect of contamination on the newly deposited underlying film on the properties of the overlying film. In addition, the length of time between presputtering a target and depositing a thin film from it was varied in order to determine the effect of target contamination on the properties of the film. Presputtering the targets prior to deposition is routinely performed in order to remove surface contaminants and atmospheric reaction products. Presputter and deposition times for the constituent thin films in several samples are shown in Table II. For Sample 9, the sequence was presputter Ti/deposit Ti/presputter Ru/deposit Ru/presputter AlN/deposit AlN. This led to a lag time of 20 minutes between deposition of two adjacent thin film layers, allowing the underlying film to react with residual gases in the chamber. For Sample 10, the sequence was presputter Ti/presputter Ru/presputter AlN/deposit Ti/deposit Ru/deposit AlN. This led to a lag time between presputtering (cleaning) the targets and using them for the actual deposition. It is possible for the targets to react with residual gases in the chamber to form oxide and/or nitride compounds on the target surface during that time. As a result, the first few monolayers of the subsequently deposited thin films may consist of a compound instead of the pure target material. Finally, Sample 11 was deposited using additional target power supplies that enabled all three targets to be presputtered

immediately prior to their depositions with no lag time between deposition of adjacent thin films. This deposition technique was used to promote compositionally pure and sharp interfaces between thin film layers.

Table 2. Presputter and deposition times for AlN//Ru//Ti thin film stacks on oxidized Si.

Sample	Ti presputter time (min.)	Ti deposition time (min)	Ru presputter time (min)	Ru deposition time	Break in deposition (hours)	AlN presputter time (min)	AlN deposition time (min)	AlN thickness (mm)	Piezoelectric response (pm/V)
1	3	7	3	21	18	20	223	2	+3.3 (xxx?)
2	10	3	10	23	0	3	223	2	0.1
3	10	3	10	21	18	10	223	2	~.5
4	10	3	10	21	0.5	10	223	2	-2.2
5	10	3	10	9	0	10	127	1	-1.29
6	10	3	10	9	0	10	127	1	-1.92
7	3	3	3	9	2	3	127	1	4.2
8	3	3	3	9	0	60	127	1	2.35
9	20	4	20	27	0	20	145	1	0.5
10	0*	4	0*	27	0	0*	145	1	-2.5
11	20†	4	20†	27	0	20†	145	1	-3.5

* All targets were presputtered prior to deposition of Ti layer.
† No lag time between presputter and deposition of thin films

The resultant samples were characterized using a variety of techniques. Piezoelectric response was measured by sectioning the samples into cantilever beams of known area and measuring deflection as a function of applied voltage at 100 Hz (xxx ask Paul C. for more details here). Crystallographic phase, orientation and average diameter perpendicular to the plane of the substrate were determined using standard θ-2θ x-ray diffraction on a Siemens D-500 XRD. Thin film topography was imaged using a high resolution Hitachi S4500 Field Emitter Gun scanning electron microscope and a Digital Instruments Nanoscope II Atomic Force Microscope. Compositional depth profiling was also performed on samples using a Cameca Secondary Ion Mass Spectroscopy (SIMS) system in order to determine the composition of the thin films as a function of depth.

In order to determine the relative dipole orientation within the AlN thin films, etch rate experiments also were performed. Sections of the AlN//Ru//Ti//SiO2//Si wafer samples were etched for times ranging from 5 to 120 minutes in a 50% nitric acid solution held at 80° C. The etched samples then were blown dry using N_2 and imaged using atomic force microscopy. The Nanoscope II contains software that calculates the root mean square (rms) surface roughness of a sample. This roughness value, combined with the detailed topological map of the sample surface, is extremely useful in determining how the surface evolves as it is etched away and the likely role of the dipole orientation. An additional sample of Ti//Ru was deposited in order to verify that the

nitric acid etch had no effect on the Ru surface or underlying Ti film. In addition, a single film of AlN was deposited directly onto an oxidized silicon wafer in order to measure the etch rate as a function of time. That the AlN was deposited onto a substrate (oxidized Si) other than that used for the samples (Ru) may have affected its crystalline and dipole orientation and consequently the resultant etch rate. Nevertheless, the measurements yielded an effective etch rate that corresponded to the time required to achieve a consistent rms surface roughness from the AFM images.

Results and Discussion for AlN Films

The piezoelectric response for each of the Ti//Ru//AlN samples is shown in Table II. For samples in which there was a lag time between deposition of adjacent thin film layers, in particular between deposition of the Ru and AlN thin film layers ($\geq$ 0.5 hours), the piezoelectric response tended to positive values (e.g. Samples 7, 8 and 9). Exposure of the pristine Ru thin film surface to residual gases in the vacuum chamber likely resulted in oxidation of the Ru surface. Although the resultant RuO_2 layer was probably limited to the first few monolayers of the surface, it appears to have been sufficiently thick to affect crystalline and dipole orientation of the subsequently deposited AlN. SIMS analysis of Sample 1 which had an 18 hour lag time between deposition of the Ru and AlN is shown in Figure 1. The results show a high oxygen-to-aluminum concentration ratio at the Ru//AlN interface (sputter time $\approx$ 1,200 seconds), suggesting the presence of an RuO_2 layer. Crystalline and dipole orientations of subsequently deposited thin film layers can be dramatically affected by this change in composition at the interface as a result of the "substrate"/thin film atomic interactions. This effect is well-documented by numerous epitaxial growth experiments. Subsequent deposition of the AlN on the oxidized Ru surface resulted in preferential dipole orientation of the AlN in the "positive" sense. The second SIMS peak showing a high oxygen-to-aluminum concentration ratio (sputter time $\approx$ 1,800 seconds) for this sample corresponds to the thermal oxide layer on the silicon substrate.

For samples in which there was a lag time between presputtering (cleaning) of the targets and the actual deposition, but minimal lag times (< 20 minutes) between deposition of adjacent thin film layers, the piezoelectric response tended to negative values (Samples 5, 6 and 10). The lag time between cleaning the targets and the depositions may have resulted in reaction at the target surfaces. Therefore, the first several monolayers of thin film deposition may have consisted of an oxide or nitride, rather than the original pure target material. In other words, the first few monolayers of Ti deposition actually may have consisted of TiO_2 instead of pure Ti. However, the short lag times between deposition of adjacent thin film layers resulted in minimal reaction of the newly deposited thin film surfaces. Therefore, for these samples, the AlN thin film was deposited onto a relatively pristine Ru surface instead of RuO_2. This is supported by the SIMS data shown in Figure 1. The only region showing a high oxygen-to-aluminum concentration ratio (sputter time $\approx$ 1,700 seconds) for this sample corresponds to the thermal oxide layer on the silicon substrate. Subsequent deposition of the AlN on the pristine Ru surface resulted in preferential dipole orientation of the AlN in the "negative" sense.

Etch rate experiments were conducted in conjunction with these samples in order to determine the dipole orientation as a function of deposition conditions. Previous researchers have reported the ability to determine the dipole orientation within crystalline $LiNbO_3$ by the relative etch rates of the opposite surfaces. Due to the different bonding conditions for the opposite dipole orientations, one dipole configuration exhibits a higher etch rate than the other. We observed a similar behavior in reactively sputtered AlN thin films. A highly oriented, crystalline AlN sample shows a relatively rough surface (rms surface roughness = 5.85 nm) in the as-deposited condition when imaged using atomic force microscopy. The surface of the sample becomes progressively smoother when it is etched for 5 and 10 minutes (rms = 4.15 nm and 1.18 nm, respectively), but then becomes rougher when etched for 15 minutes (rms = 2.93 nm). A possible explanation for this is that one of the two dipole orientations has a relatively faster growth and etch rate than the other. Its faster growth rate results in an uneven, rough surface as shown schematically for the as-deposited sample in the figure. As the sample is etched, the relatively tall peaks are preferentially etched away until the sample is very smooth, as shown in the figure of the 10 minute etch time. With continued preferential etching of those grains, their surfaces subside below those of the surrounding, more chemically resistant grains. As a result, the surface begins to roughen again, as shown in the figure of the 15 minute etch time.

Ultimately, as the AlN film is etched away completely, the rms roughness of the sample approaches that of the as-deposited underlying Ru thin film (2.2 nm). Etching experiments performed on a Ti//Ru stack showed that the overall appearance and roughness of the electrode stack did not change appreciably for etch times of up to 180 minutes. This indicates that the changes in the appearance of Ti//Ru//AlN samples with etching can be attributed to etching of the AlN film only. In addition, a single thin film of AlN deposited on a silicon substrate was determined to have an average etch rate of 32 nm/min. That means that a 1 micron thin AlN thin film should be completely etched away in approximately 31 minutes. The AFM images for most AlN samples showed little change for etch times beyond 40-50 minutes, suggesting that the AlN thin film had been etched away by that time and the chemically resistant Ru electrode layer was exposed at the surface. That the AlN thin film etches unevenly as shown in Figure 2 suggests preferential etching of a particular crystallographic or dipole orientation. X-ray diffraction of these samples showed strong preferential orientation of the AlN (0002) hexagonal net of atoms parallel to the plane of the substrate. Given the highly oriented crystallographic nature of this sample, it is possible that the increased roughness may result from preferential etching of one of the two dipole orientations commensurate with that crystallographic orientation.

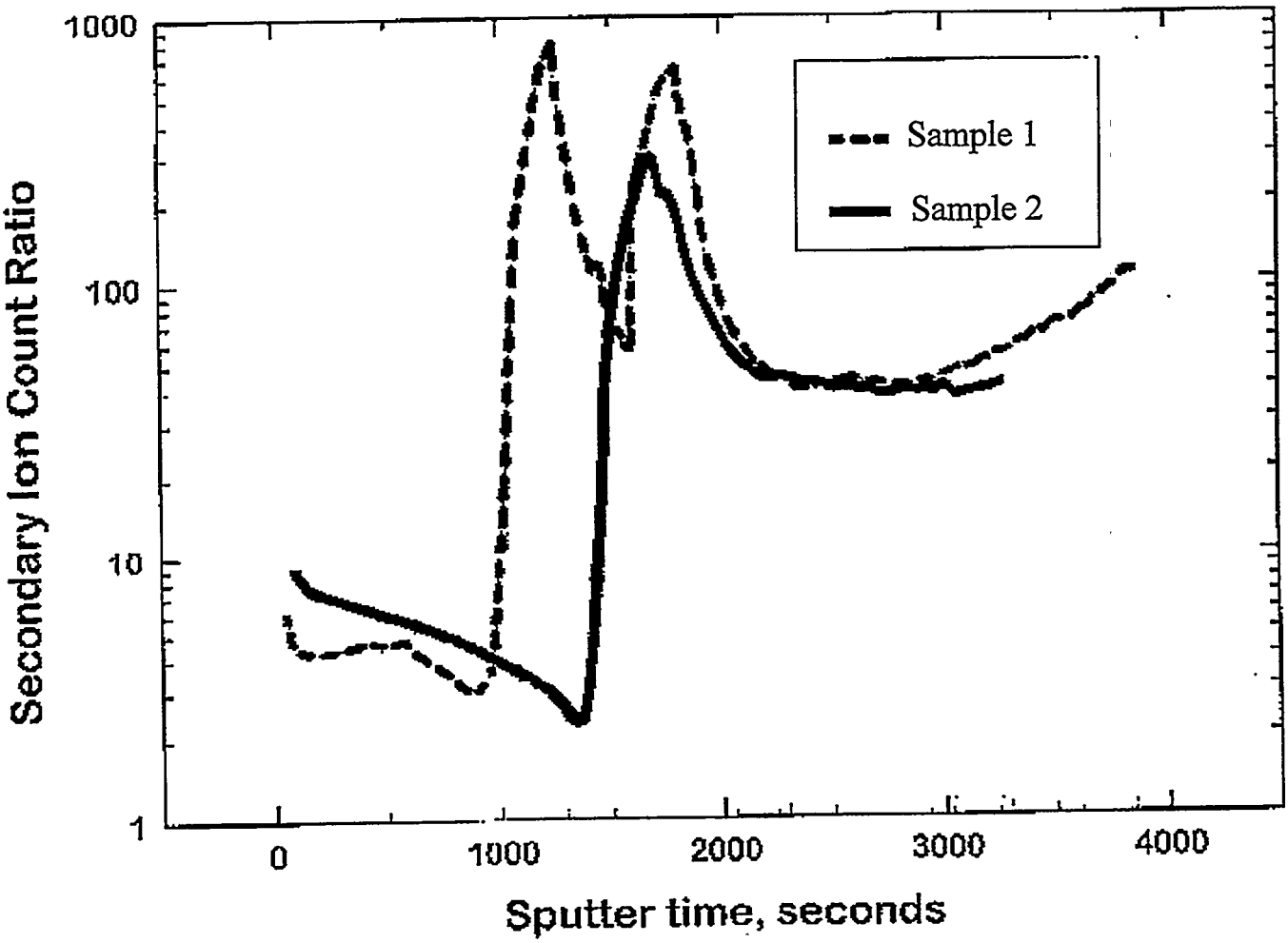

Figure 1 . SIMS data for two Ti//Ru//AlN samples showing regions of high oxygen-to-aluminum concentration ratios for samples with and without a break between Ru and AlN depositions (Samples 1 and 2, respectively).

PZT Thin Films

$Pb(Zr,Ti)O_3$ thin films were investigated for FPW devices because of their exceedingly high piezoelectric response. Piezoelectric coefficients 500 times greater than quartz and 130 times greater than GaAs have been achieved in suitably doped, bulk PZT materials. In this program, we developed PZT thin films that had piezoelectric coefficients that were 200 times greater than quartz and 50 times greater than GaAs. The reduction in piezoelectric response compared to bulk materials is due to clamping of 90 type domain walls due to misfit dislocations at film // substrate interfaces.[1] During the course of this study, a large number of different PZT films were fabricated, we will summarize the processing and characterization of only a few of these films. A summary of some of the more noteworthy PZT films fabricated for this program is shown in Table 3.

IMO refers to the inverted mixing order process for PZT thin films, [2,3] a hybrid metallorganic decomposition process (sol-gel) that Sandia has used to fabricate numerous films over the last several years. Typically 0.1 μm thick layers are deposited, with crystallization treatments (550 C to 650 C) being employed after every 4 layers. The diol process [4,5] has the advantage that thicker films can be deposited in a single layer, as thick as 0.5 μm. Because of the high dielectric constant, the impedance of the PZT thin film devices in a ground plane structure leads to low impedance and thus difficulty in obtaining reasonable acoustic response. This recurring theme will be discussed in detail in the device characterization section.

IMO PZT 53/47 Thin Films

The electrical property measurements of four PZT 53/47 films fabricated for the flexural plate wave (FPW) microsensor project is described. The film sections for our electrical measurements were taken from individual 3" wafers before the remainder of the wafers were processed into surface acoustic wave (SAW) devices. In summary, these films fabricated by Dept. 1492 are either 1.2 μm (12 layers) or 2.0 μm (20 layers) thick and are representative of Sandia's best films. Dielectric constants on the order of 1200, well defined, low loss hysteresis loops and saturated polarizations on the order of 49 $\mu C/cm^2$ were measured. In addition, we performed direct piezoelectric measurements (modified Berlincourt meter) on the films by application of a 0.2 Nt force at 100 Hz and measured d_{33} piezoelectric coefficients on the order of 90 pC/Nt.

Table 3. Processing and composition of PZT thin films

Film Composition	Thickness	Substrate	Devices / Process
PZT 53/47	1.2 μm, 2.0 μm	Pt//Ti//Si, LSCO//Ti//Si	SAW / IMO; good piezo properties, little acoustic response due to impedance
PNZT 2/53/47	1.2 μm, 2.0 μm	ibid	ibid
PZT 40/60	0.8 μm	Pt//Ti//SiO_2 //SiN	Bulk micromachined cantilever beam / Diol; approximately 100 pM/V d_{33} measured
PZT 40/60	1.2 μm, 2.0 μm	$LaAlO_3$	SAW 58 MHz to 168 MHz SAW / IMO; no acoustic response
PNZT 2/40/60	1.2 μm	$LaAlO_3$	Ibid, SAW response; Q =28
PZT 40/60	1.2 μm	ZrO_2 // Si	SAW, sample surface too rough to deposit IDE
PNZT 2/40/60	1.2 μm	ZrO_2 // Si	ibid
PNZT 2/52/48	1.2 μm	ZrO_2 //Si	ibid
PZT52/48	1.2 μm	Cr//Au//PZT//Pt//Ti/ /poly Si FPW	surface micromachined Si; Hysteresis loop obtained, Pr = 18 $\mu C/cm^2$

Electrode Deposition:

Electrodes for these capacitors were sputter deposited by Dept. 1812. Four different films were processed on 3" diameter wafers with electrode stacks of either: 100 nm LSCO // 170 nm Pt // 30 nm Ti // 40 nm SiO_2 // Si or 170 nm Pt // 30 nm Ti // SiO_2 // Si. The top electrodes (TEL) were 100 nm thick Pt and on the order of 400 μm in diameter. The 4 films investigated were:

(1) 12 layers PZT deposited on Pt coated Si
(2) 20 layers PZT deposited on Pt coated Si
(3) 12 layers PZT deposited on LSCO coated Si, and
(4) 20 layers PZT deposited on LSCO coated Si.

These films were processed at 650 C for 30 min using a heating rate of 50 C/min. The top Pt electrodes were annealed at 550 C for 10 min in air.

Dielectric Measurements:

A description of the electrical tests follows. For the polarization and Vc values, the 12 layer films and the 20 layer films with no TEL anneal were tested with a driving voltage of 40 volts peak to peak, while the 20 layer films with a TEL anneal were tested with a driving voltage of 80 volts peak to peak. These applied voltages correspond to unipolar fields of 167 kV/cm, 100 kV/cm and 200 kV/cm, respectively. These applied voltages meet the IEEE ferroelectrics standard rule of thumb for saturation in that the applied voltage is more than three times greater than the coercive voltage. Pushing the envelope, for the 2.0 μm thick - Pt sample, on one TEL dot, we obtained hysteresis loops for unipolar applied fields of 200, 250, 300, 350, 400 and 450 kV/cm. Because of the degradation of the loop at 450 kV/cm, we used a field of 350 kV/cm to obtain statistical data. A saturated polarization of 48.6 $\mu C/cm^2$ and a remanent polarization, P_R, of 25 $\mu C/cm^2$ were obtained from these measurements, as shown in Table 4. These results are comparable to our best measurements, historically. Top electrode dots on the order of 400 mm diameter were used. The dielectric constants tabulated were measured at 10 kHz and with an applied voltage of 0.1 volt rms. Dissipation factors typically ranged from 0.023 to 0.028, which is once again in good agreement with some of our best films.

Piezoelectric Measurements:

Piezoelectric measurements were made by slightly modifying the test fixture for a Berlincourt meter. For this measurement, an oscillating force head applies mechanical stress to a piezoelectric, and through the direct piezoelectric effect charge is generated on the faces of the ceramic. Obviously, the greater the charge generated per unit force, the greater the piezoelectric coefficient. For our measurements, a 100 Hz, 0.2 Nt mechanical force was applied and the piezoelectric current generated by the sample was converted into the piezoelectric d_{33} coefficient. The d_{33} notation represents a charge measurement taken in the direction of poling with the stress also being applied in this same direction. A wire was used to make electrical connection between the bottom electrode of the film and the bottom force head to permit the piezoelectric measurement. For the 20 layer LSCO sample, we tested top electrode dots of 400 mm and 2 mm dimensions. For the 400 mm dots, we tested a series of 3 top electrode dots poled in one direction and 4 other top electrode dots electrically poled in the opposite direction. The

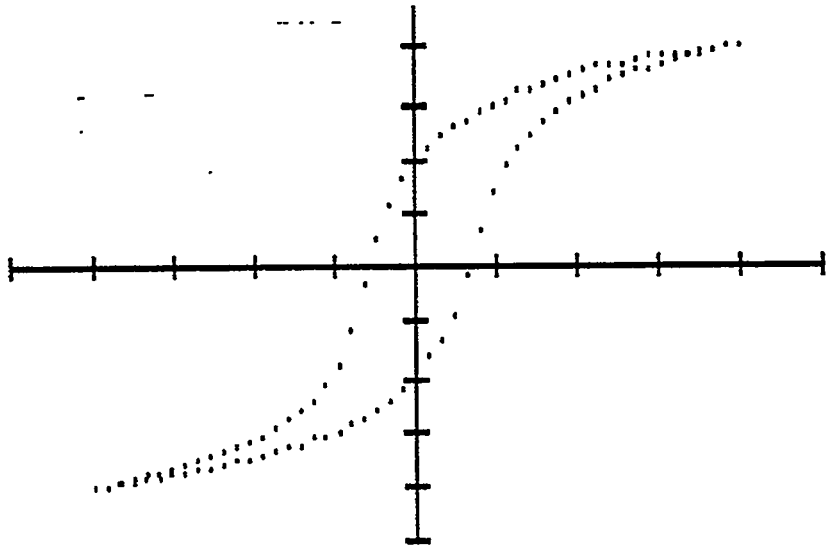

Figure 2. Dielectric hysteresis characteristic for a PZT 53/47//LSCO//Pt//Ti//Si film. (Y-axis: Polarization (11 $\mu C/cm^2$/div); X-axis: Volts (5 volts/div))

Table 4. Dielectric Properties of SAW PZT 53/47 Films

Film Description	Ps ($\mu C/cm^2$)	Pr ($\mu C/cm^2$)	Vc (volts)	Dielectric Constant (10 kHz)
12 layer Pt No TEL Anneal	40.6 ± 2.1	20.0 ± 1.2	3.34 ± .03	1201 ± 50
12 layer LSCO No TEL Anneal	41.5 ± 1.2	22.0 ± 0.8	3.47 ± .04	1109 ± 94
20 layer Pt* No TEL Anneal	33.9 ± 1.6	18.5 ± 1.1	5.01 ± 0.1	1226 ± 49
20LayerLSCO* No TEL Anneal	36.4 ± 2.6	20.9 ± 1.6	5.15 ± .01	1217 ± 101
12 layer Pt TEL Anneal	40.5 ± 1.8	20.3 ± 1.0	3.13 ± 0.03	1309 ± 50
12 layer LSCO TEL Anneal	44.8 ± 1.7	21.5 ± 0.8	3.04 ± 0.04	1426 ± 34
20 layer Pt TEL Anneal	41.1 ± 1.3	20.4 ± 0.7	5.09 ± .10	1320 ± 40
20 Layer LSCO TEL Anneal	42.1 ± 3.0	20.4 ± 1.3	4.81 ± .04	1241 ± 144
20 layer Pt** TEL Anneal	48.6 ± 2.7	25.2 ± 1.7	5.89 ± .07	N/A

* ±20 volts applied
** ±70 volts applied

sign of the piezoelectric coefficient was consistent with, and changed with, the direction of electric field poling. To further confirm that we were truly measuring a film response and not some artifact of the underlying electrode // Si wafer technology, we tested an electrically depoled sample. Electrical depoling means that we brought the macroscopic remanent polarization of the film to zero. Piezoelectric coefficients less than 9 pC/Nt were measured in all but one case after depoling. For the 20 layer PZT // LSCO film that had 400 μm diameter electrodes and was poled at 40 volts for 5 seconds at ambient, we measured d_{33} values of -54 ± 8 pC/Nt and +73 ± 17 pC/Nt.

Piezoelectric tests on the 2 mm X 2 mm electrodes provided slightly different results which we believe are more accurate than the small area electrode measurements. All eight of the 2 mm X 2 mm electrodes provided excellent dielectric properties, implying large area yield, perhaps appropriate for SAW measurements. Our test sequence for the 2 mm X 2 mm electrodes was as follows: samples were poled at 40 volts for 5 seconds and then d_{33} measured, the samples were then poled at 50 volts for 2 seconds and d_{33} measured, the samples were electrically depoled as confirmed by single shot hysteresis and then d_{33} measured. Finally, another single shot hysteresis loop was taken to confirm that the remanent polarization was less than 3 $\mu C/cm^2$. The average d_{33} after 40 volt poling was 86.8 ± 7.9 pC/Nt, the d_{33} after 50 volt poling was 91.6 ± 4.6 pC/Nt and the d_{33} after depoling was 8.0 ± 4.9 pC/Nt. The results are summarized in Table 5.

Table 5. Piezoelectric measurements for the 2.0 μm thick PZT // LSCO film

Dot Number	d_{33} (pC/Nt) 40 volts	d_{33} (pC/Nt) 50 volts	d_{33} (pC/Nt) Depoled
1	-95	Breakdown @ 60 V	
2	-91	-95	Breakdown
3	-95	-97	-4
4	+78	+91	+8
5	+82	+88	+4
6	+80	+85	+8
8		-93	+6
7			+17

Device Fabrication Methods and Process Development

Surface micromachining methods

The surface micromachining process for silicon-based FPW's is summarized in Fig. 3. Shallow cavities are etched into the silicon substrate and lined with silicon nitride. The cavities are overfilled with deposited (sacrificial) oxide layers. Chemo-mechanical polishing (CMP) then planarizes the surface. Low-stress silicon nitride is deposited and patterned with etch release holes that allow removal of the sacrificial oxide. After the etch release, the membranes are sealed with another LPCVD low-stress nitride layer.

Since some of these piezoelectric materials (PZT and ZnO) are not allowed in the MDL due to contamination issues, the additional processing required to fabricate a piezoelectrically driven FPW was to be done in the CSRL and associated processing facilities. The surface micromachined devices were included as part of a mask set for 150-mm wafers encompassing several other projects. Completion of the piezoelectric devices required an additional set of masks compatible with the 75-mm wafer processsing capabilities of the CSRL facilities. Processing of the piezoelectric stack was to be completed on small pieces of the original 150-mm wafers.

Bulk micromachining methods

A bulk micromachined process was also developed and appropriate masks designed and obtained for both mag-FPW's and piezoelectric FPW's. The basic process flow is described schematically in Fig. 5. The bulk micromachined FPW process begins with a double side polished, <100> silicon wafer coated on both sides with low-pressure chemical vapor deposited (LPCVD) low-stress nitride. The nitride acts as both the base membrane material and the KOH etch mask. For piezoelectric actuation, the ground plane and piezoelectric material stack is deposited on the front side before any patterning is done. Then the backside nitride window is defined and opened. The front transducer patterns are defined and aligned to the backside windows. Finally, the silicon is etched away to release the membrane. The nitride windows must be precisely oriented with respect to the <110> planes of the <100> silicon wafer to maintain control over the membrane size and the transducer-to-membrane alignment. Black wax or a protective chuck must be used to protect materials not compatible with the KOH solution (e.g. Al metalization, PZT stacks...).

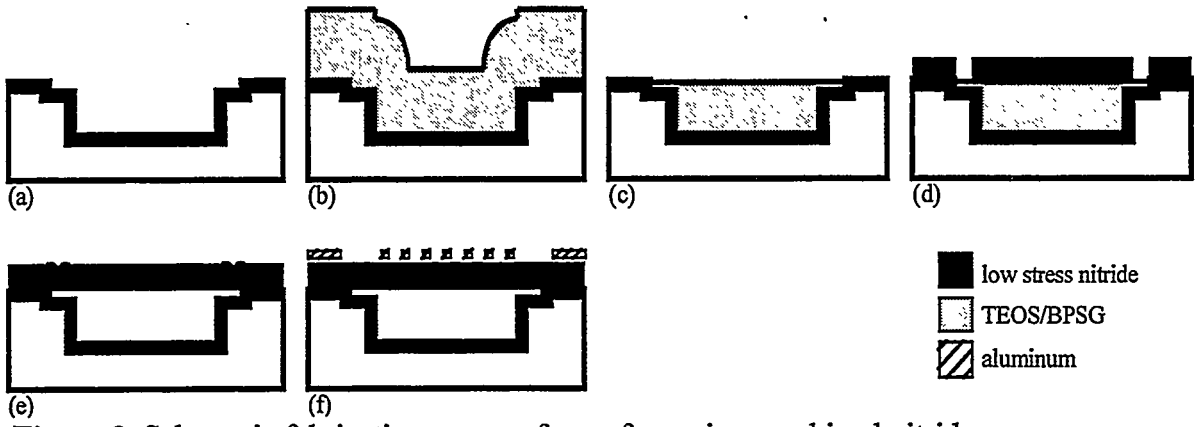

Figure 3 Schematic fabrication process for surface micromachined nitride membrane FPW sensor. Dimensions are not to scale. (a) Etch two separate patterns in substrate and deposit nitride liner/polish stop. (b) Deposit thin oxide (BPSG) and thick oxide (TEOS). (c) Polish oxide stack to planarize the surface. (d) Deposit diaphragm nitride, and pattern release etch holes. (e) Release etch diaphragm and seal with nitride. (f) Deposit and pattern aluminum.

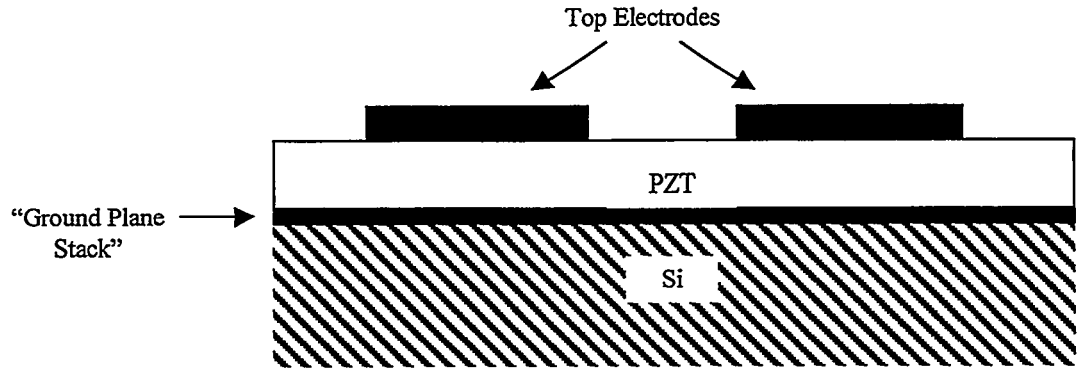

Figure 4. First-generation SAW designs wuth conductive ground plane. The drawing is not to scale. The thickness of the PZT layer ($\approx$ 1 μm) is much less than the spacing between the IDT fingers (several tens of microns), therefore the electric field is dropped directly under the fingers to the ground plane rather than to adjacent fingers. One comb (normally grounded) was thus eliminated from the first generation IDT's. The ground plane serves to increase the coupling to the peizoelectric film and acts as a template for growth of the highly oriented PZT film.

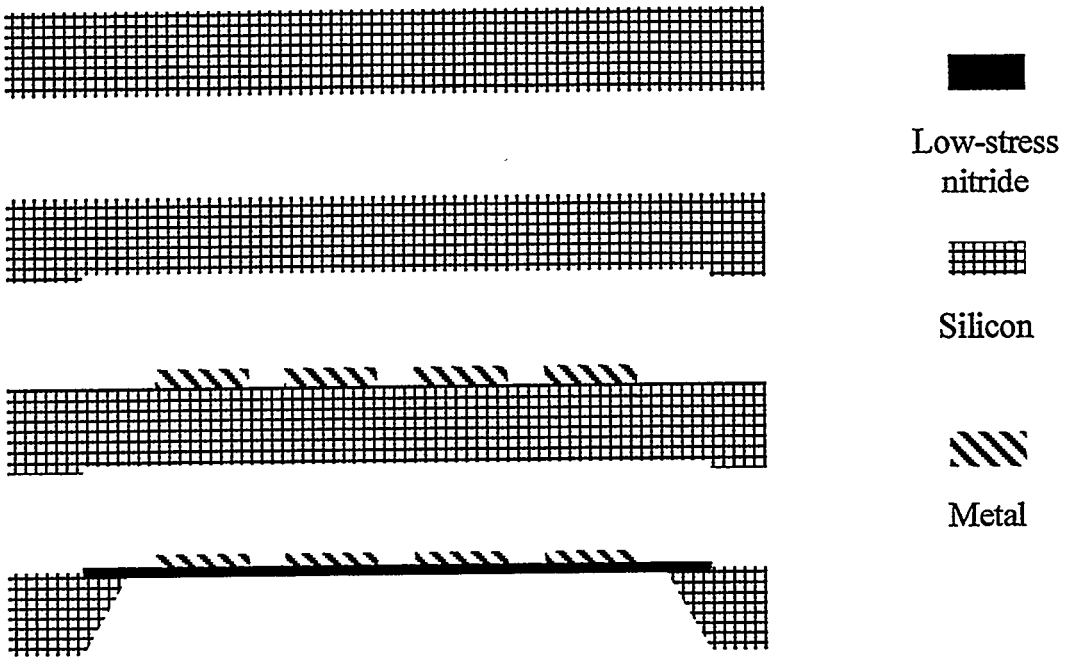

Figure 4. Schematic representation of the bulk micromachined mag-FPW process. From top to bottom, one starts with a <100> Si wafer polished and coated on both sides with low-stress silicon nitride ranging up to 2 μm thick. A window is patterned in the LSN on the backside, carefully aligned to the major flat of the wafer using a patterned photoresist (not shown) and a dry etch. Blanket metal coverage is put down (not shown) and patterned using patterned resist and an appropriate metal etch, aligned precisely to the windows in the LSN on the back side of the wafer. Finally the silicon is removed from the backside of the wafer using an anisotropic Si etch (e.g. KOH). Depending on the metalization used, it may need to be protected by black wax during the KOH etch. The piezoelectric FPW device process is the same except that the several additional layers (60-nm SiO_2/ Ti /TiO_2/Pt/PZT or an equivalent stack for AlN) are required before the top metal layer is deposited. We deposited these layers before defining the backside windows in the LSN. The piezoelectric stack had to be protected by black wax while immersed in the KOH solution.

Metalization patterning for piezoelectric thin-film devices

Patterning of the transducers must be compatible with the underlying materials in the piezoelectric stack. Compatibility issues are simplified when liftoff patterning methods are used. Alternatively, blanket transducer metals can be deposited and patterned using appropriate wet etches. Liftoff was used with both Ti/Pt and Cr/Au transducer metalizations, while wet etching was used only on the Cr/Au.

Liftoff Metal Patterning

As mentioned above, metal patterning by photoresist liftoff is the preferred method due to concerns about the reaction between the piezoelectric layers and the acid etchants used for metal definition. Wafers with the piezoelectric thin-films already deposited were spin coated with AZ 5214 photoresist at 5 K PRM for 30 sec. Following a 90°C, 90 sec. soft bake on a hotplate, the positive image pattern was exposed on a contact aligner, the wafer was baked at 112°C for 45 sec. and then flood exposed on a contact aligner for 45 sec. The reverse imaged wafer was then developed in AZ 312 developer at a 1:1.4 concentration, rinsed, and dried. A 30-minute UV/ozone treatment at room temperature was done immediately before metalization to insure good metal adhesion to the surface. Metal deposition was done in a dual e-beam evaporative system for the Cr/Au metal and in a sputter deposition system for the Ti/Pt metal. Following the metal deposition, the wafers were soaked in acetone for periods of time ranging from several hours to several days, followed by sonic agitation in acetone and acetone high pressure spray to remove the metal/photoresist. Problems with this process resulted from large particles in the PZT layer. The particles prevented good contact between the mask and wafer in the exposure step. This lead to defects in the pattern that caused opens or shorts between metal lines and in extreme cases gross deformation of the desired patterning.

Wet Etch Metal Patterning

Due to the patterning problems with the liftoff process, the effects of the metal etchants on PZT piezoelectric properties were evaluated. Blanket PZT layers were exposed to photoresist coating and solvent stripping and Cr and Au etchants, then electrically evaluated with shadow mask formed dot capacitors. No degradation of the PZT performance was noted. The wet etching process, the Cr/Au metal was blanket deposited on the PZT surface following a UV/ozone clean for 30 min. at room temperature immediately prior to deposition. The wafers were then coated with AZ 4330 photoresist at 5 K RPM for 30 sec, followed by a 90 C, 90 sec. soft bake on a hotplate. The positive image pattern was exposed on contact aligner for 7 sec, and developed in AZ 400K developer at 1:4 dilution. The Au metal was then etched in an I2/KI/H2O solution for 15 sec. The Cr was etched in a cerric ammonium nitrate/nitric acid/water solution for 18 s. The photoresist mask was stripped in acetone followed by methanol.

Device Designs

Thin-film SAW devices

Thin-film surface acoustic wave (SAW) devices were included in the project as useful and instructive devices that are easier to fabricate than FPW devices. SAW fabrication is simpler and faster because there are no silicon micromachining steps.

With ground plane

Surface acoustic wave (SAW) devices made on bulk piezoelectric materials like quartz or lithium-niobate, commonly use interdigitate electrodes (IDT's) to launch the acoustic wave. The IDT is made up of two combs offset from each other by a half wavelength so that the fingers are interdigitated. Two-port devices use one IDT to launch the wave and a second to receive it after it has traveled some distance through the substrate.

Over the course of the project, two different mask designs were done for piezoelectric thin-film SAW devices to be made on Si substrates. A range of wavelengths was chosen to be compatible with existing testing hardware within the Microsensor R&D Department for quartz-based SAW sensors. The nominal frequencies indicated are based upon theoretical descriptions of thin film PZT devices published by Shih and Wu. [7] To calculate these frequencies PZT film thicknesses ranged from 1.2 to 3.0 μm. The film thickness and wavelength affect the phase velocity as indicated in Figure 10 of the paper by Shih and Wu. Thicker PZT films lower the phase velocity below that of silicon, while wider finger spacing (longer wavelength) tends to increase the phase velocity.

The first generation SAW design utilized a ground plane below the SAW transducer as shown in Fig. 4. With PZT films, this ground plane serves not only to increase the coupling into the piezoelectric films, but also acts as a template for deposition of highly oriented PZT films. Because the piezoelectric film thickness is much less than the transducer wavelength, and the field is therefore much higher between the fingers and the ground plane than between adjacent fingers. One set of fingers (comb) can be eliminated (reference the Purdue thesis). When a ground plane is used, all of the devices we fabricated are expected to have coupling coefficients at least as good as that of quartz according to the Shih and Wu results.

Without ground plane

A second generation SAW design was pursued because PZT devices using the first generation design suffered from extremely high parallel plate capacitance between the fingers and the ground plane. The high capacitance issue is peculiar to the PZT devices because of their extremely high dielectric coefficients ($600 < \varepsilon < 1000$) in comparison to other piezo films like ZnO and AlN ($\varepsilon \approx 10$). The capacitance effectively shorts the devices as higher frequencies (> 10 MHz). The second-generation design minimized the capacitance by eliminating the conductive ground plane and including both sets of IDT

fingers in the transducers. An electrically insulating template layer (ZrO) was used to improve the PZT film quality. Other device parameters were kept the same between the two SAW generations. Poling fields for the second generation devices were about an order of magnitude higher than for first generation devices because of the increased distances.

FPW Devices

Flexural plate wave (FPW) devices were designed for both magnetic excitation and piezoelectric excitation of the acoustic wave. Magnetically excited devices, called mag-FPW's here, use Lorentz forces on alternating current lines on the membrane to set up the wave. Piezoelectric excitation requires IDT's similar to those described for the SAW devices above. In addition to the different excitation mechanisms, the project included both surface and bulk micromachined devices. An example of a 2-port magnetic resonator is shown in Figure 6. [7]

Surface micromachined

Designs for several versions of surface micromachined FPW's were developed for processing in the MDL. These devices were based on the MDL technology of 1996, using low-stress silicon nitride (LSN) or low-stress polysilicon (LSP) as the membrane layer. Both single and dual port FPW delay lines and resonators were included in the MDL mask set. Delay line devices used a trapezoidal membrane (slanted ends) to kill edge reflections, while the resonators used rectangular membranes with precisely positioned transducers to set up a standing wave. Both types were designed with 4, 6, or 8 finger pairs in the transducers. The transducers used an 8-μm period with 2-μm finger widths and spaces. The membranes ranged up to a few hundred microns on a side. Depending on the residual stress in the composite membrane structure of the finished devices, the operating frequencies were expected to be around 5 MHz.

Magnetic actuation

Bulk micromachined

Only resonator structures were included in the bulk micromachined FPW masks for both piezoelectric and magnetic actuation. Generally the bulk devices were much larger than the surface micromachined devices (wavelengths to 400 μm and membranes up to 5000 μm on a side). Depending on the membrane thickness and tension, resonance frequencies were expected to range from a few hundred kHz to a few MHz.

Piezoelectric actuation

Piezoelectrically driven FPW devices utilize interdigitated electrodes similar to the SAW delay line device. However, resonator FPW devices typically have fewer finger pairs in the transducers than a SAW delay line transducer (4-8 pairs instead of 25-50 pairs), and smaller transducer separation (only a few acoustic wavelengths rather than 10's to 100's of wavelengths). Transducers with either four or six finger pairs were used. Wavelengths were either 246 or 320 μm. Transducer separation was either one or two acoustic wavelengths. In addition, the transducers are accurately located with respect to

the membrane edges so that the metal lines will lie at the antinode (maximum displacement) locations with respect to the membrane edges (clamped nodes).

Magnetic actuation

The basic design rules for the mag-FPW devices is the same as for the piezoelectrically excited devices except that a meander line transducer is substituted for an interdigitated transducer. The bulk micromachined mag-FPW's used the same wavelengths and transducer sizes as their piezoelectric counterparts.

Cantilever devices

Cantilever beam devices were fabricated by several different procedures during the course of this study [8,9] to characterize the piezoelectric properties of both PZT and AlN thin film materials. Macro-cantilever beams were fabricated using no photolithographic procedures, typically dimensions of a device were 1 cm length X 1.5 mm width. The underlying substrate was 300 mm thick Si. The cantilever beams were typically driven by a triangular waveform voltage of 2 volt to 6 volt amplitude and at frequencies ranging from 50 Hz to 4000 Hz. Deflection of the cantilever beam as a function of applied voltage was monitored using a MTI-200 fotonic sensor (fiber optic array). From this deflection the piezoelectric d_{31} coefficients of the films could be calculated.

$$d_{31} = (dt / (E*3))* (Y(Si)/Y(PZT))*(h_{sub}^2/ L^2)* (1/h_{film}) \quad (1)$$

Where dt is the deflection of the end of the cantilever beam, Y(PZT) is Young's modulus of thePZT, Y(Si) is the Young's modulus of the Si, E is the electric field, hsub is the thickness of the substrate, L is the length of the beam and hfilm is the thickness of the piezoelectric film. From these measurements, d_{33} coefficients of 8.9 pM/volt were obtained for highly c-domain oriented AlN films, in reasonable agreement with single crystal values. A d_{33} coefficient of 90 pM/Volt was obtained for PNZT 52/48 thin films, about half the value of the bulk piezoelectric materials. The PNZT result is consistent with findings of other research groups through out the world and is due to clamping of 90 domains at the substrate interface by misfit dislocations. Nonetheless, a piezoelectric coefficient value of 90 pM/V is 60 time s greater than that of GaAs and 150 times greater than that of quartz. In addition to the macrocantilever beams, bulk Si micromachined, piezolectric thin film microcantilever beam devices were fabricated in this study with PZT thin films. Typical dimensions of the microcantilever beams ranged from 100 mm wide by 100 mm to 800 mm long. A nine step process was initially developed to fabricate the SiN//PZT thin film devices. Critical processing steps included development of a 60 nm sputter deposited SiO_2 layer on the SiN to enhance adhesion of the underlying Ti// Pt electrode to this structure. A second process improvement was the photolithographic definition of the PZT films so that they did not come in contact with the underlying SiN during the high temperature (550 C to 650 C) crystallization treatments. Both the piezoelectric and dielectric responses of these integrated piezoelectric thin film structures were consistent with previous tests of macrocantilever beams.

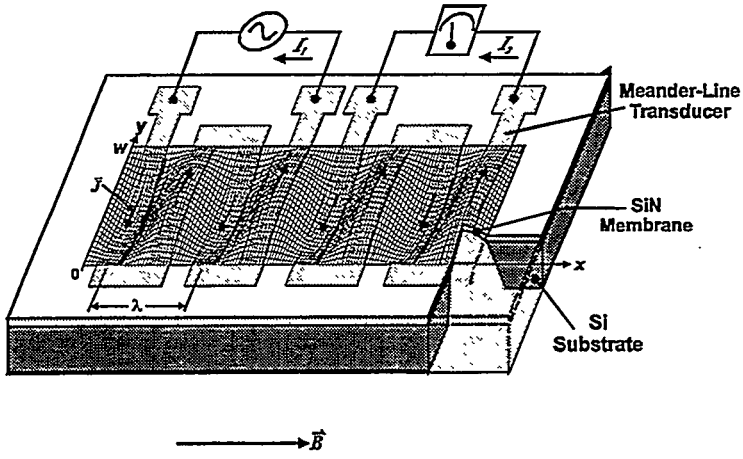

Figure 6. Schematic representation of a 2-port mag-FPW resonator. The Lorentz force interaction between the alternating current and the static in-plane magnetic field forces adjacent legs in the transducer to move in opposite directions.

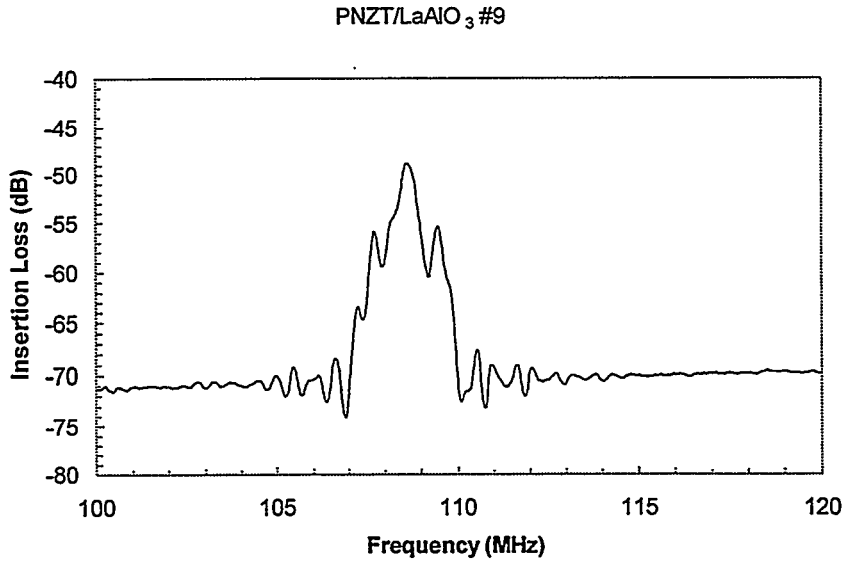

Figure 7. Results of a transmission measurement on a PNZT-on-$LaAlO_3$ SAW device. This particular device had a transducer wavelength of 64 μm and a path length between the transducers of 120 wavelengths.

Device Characterization

Electrical Poling of PZT Thin Films

Electrical poling of PZT thin films was achieved on both ground plane devices and interdigitated devices with no ground plane. For the devices with ground planes approximately 300 kV/cm was applied for 30 seconds. Since film thickness varied between 0.8 μm and 2.0 μm in this study, voltages of 24 volts to 60 volts were used. Devices that did not have a conducting ground plane required much greater voltages to electrically pole the PZT films due to the considerably greater separation between transducer fingers (250 μm to 320 μm). Initial attempts to pole the devices in air were not succesful, because of electrical breakdown along the PZT film surface. A procedure was developed to pole the films in fluorinert. Single shot dielectric hysteresis loops confirmed that the interdigitated devices were indeed poled. Well saturated hysteresis loops with remanent polarization values on the order of 20 $\mu C/cm^2$ were obtained with application of 600 volts.

Acoustic Measurements

The SAW and FPW devices were characterized electrically using a Hewlett-Packard network analyzer (8753C or an 8751A). Single-port devices, where the same port must be used for input power and output signal, were characterized in the reflection mode. Both the magnitude and phase of the signal can be measured as the drive frequency is swept slowly through the resonance. When away from resonance, most of the input power is reflected back out of the device. At resonance, the power is effectively coupled into the device and strong dip in the reflected power is observed, along with a small phase shift. Basically, a sharp impedance variation occurs at the resonance. The amplitude and half-width of the impedance variation are a measure of the device quality, typically defined by a quality factor Q (defined as the resonance frequency divided by the bandwidth 3 dB down from the peak value). The phase shift in a one-port device is generally so small that it is not useful in sensor applications.

Two-port devices use one port to drive the device and a second port to pick up the regenerated signal after the acoustic wave travels a certain path length. The network analyzer is used to make a transmission measurement. Again the frequency is swept through the resonance condition. Out of resonance, almost all power should be reflected (i.e. the insertion loss should be high – no throughput). At resonance, power is efficiently coupled into the device and the output power becomes a significant fraction of the input power. Two-port devices give 180° phase shifts at the resonance condition.

SAW Devices On Si

Our initial attempts to fabricate piezoelectric thin-film SAWs on silicon involved the use of AlN or PZNT films with appropriate ground planes. None of these devices were functional. The AlN devices failed for reasons discussed above in the thin-film materials section. The PNZT devices failed because of the high parallel plate capacitance arising from the high dielectric constant of the film. Subsequently, for PNZT devices we changed to a second device design that eliminated the conducting ground plane. ZrO_2 sputter deposited thin films were used as the template and diffusion barrier to the underlying SiO_2 for the PNZT deposition. As this technology was not as well developed at Sandia as the use of the Pt ground plane, we also tested PNZT films on single crystal $LaAlO_3$ substrates. These electrically insulating substrates also work well as a growth template.

SAW Devices On $LaAlO_3$

Functional SAW devices were fabricated on $LaAlO_3$ in two different lots. Electrical yield was on the order of 20-30%. Furthermore, substantial variability in insertion loss for nominally identical devices was observed. Figure 6 shows the insertion loss measured for a SAW device with 64-μm wavelength and 120 wavelengths between the input and output transducers. The main peak is centered at about 108 MHz and shows some structure due to edge reflections. Note that this measurement was done without impedance matching to improve the coupling of power into the device.

Table 7 summarizes the average results on PNZT SAWs fabricated on $LaAlO_3$ substrates. The resonant frequency depends upon the wavelength in the expected fashion. All of the functional devices indicated an acoustic phase velocity of about 7000 m/s. This number should approach the surface wave velocity of the $LaAlO_3$ substrate.

Table 7. SAW characteristics of PNZT//$LaAlO_3$ devices

Acoustic Wavelength (μm)	**PNZT Thickness (μm)**	**Resonant Frequency (MHz)**	**Calculated Phase Velocity (m/s)**
120	1.2	59.5	7140
64	1.2	108	6910
40	1.2	173	6920
28	1.2	No yield	-

SAW Devices On silicon

Acoustic resonances were observed in the PNZT/ZrO_2 /Si SAW devices fabricated at the same time as the PNZT/$LaAlO_3$ devices discussed above (Figure 7). However, unlike the devices on $LaAlO_3$, the resonant frequencies did not scale as expected with the transducer wavelength. Figure 7 shows the insertion loss measured with two different SAW devices having wavelengths of 120 and 64 μm. Both of these devices resonated around 125 MHz. In addition, both devices showed a series of oscillations spread out over about 50 MHz, centered around 200 MHz. Other devices of this type with wavelengths of 40 μm displayed very weak resonances at about 180 MHz.

Surface micromachined FPW Devices

Functional surface micromachined FPW devices of either piezoelectric or magnetic actuation types were never fabricated. Released and sealed MDL membranes were fully deflected (pinned to the bottom of the underlying, evacuated cavity) by atmospheric pressure. The fully deflected membrane eliminated testing of the mag-FPW devices in the MDL mask set, made it difficult to deposit high quality piezoelectric films onto the uneven surface, and prevented definition of the final metal layers. However, we were able to deposit 1.2 μm thick PZT thin films on surface micromachined, poly Si membraned FPW devices. The initial Al electrodes were etched off and replaced by a Ti//Pt electrode stack upon which the PZT films were deposited. Cr//Au interdigitated electrodes with 64 μm pitch were deposited on the PZT film and then defined by chemical etching, which was shown in preliminary tests to not drastically alter the PZT film properties. Remanent polarizations on the order of 14 $\mu C/cm^2$ were measured, about half the value for films on blanket wafers. The deflection of the membranes after fabrication was postulated to be the cause of this degradation. Because of the high capacitance of the PZT devices, a low impedance was obtained at high frequencies making measurement of acoustic response impossible.

Bulk micromachined FPW Devices

Although complete devices were fabricated, we were unable to detect acoustic resonances in any of the piezoelectrically actuated FPW devices. The high parallel plate capacitance of the PNZT devices appears to shunt these devices just as it did the SAW devices using the ground plane.

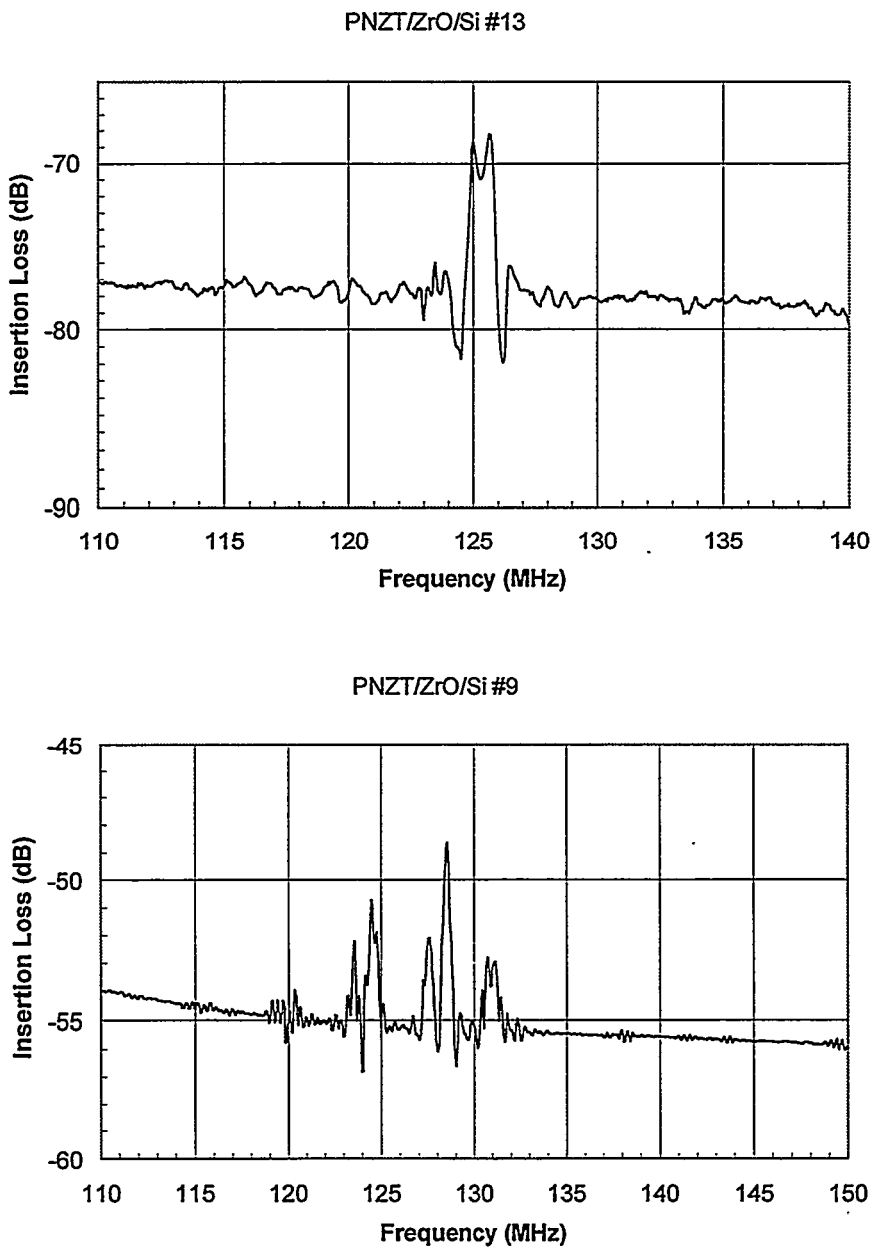

Figure 8. Results of transmission measurements on PNZT/ZrO_2/Si SAW devices. Note that despite the different wavelengths, the resonant frequency of the devices is essentially unchanged. Device #13 has a wavelength of 64 μm while device # 9 has a wavelength of 120 μm. The multiple resonances (especially apparent in the lower trace) may indicate complicated acoustic modes involving reflections at the various layer interfaces.

Summary

A unique meshing of the following technologies was developed from this piezoelectric thin film // flexural plate wave LDRD:

(1) Si surface micromachining,
(2) bulk Si micromachining,
(3) PZT thin film integration and
(4) high quality AlN film deposition.

Among the highlights of the program were the deposition and dielectric characterization of PZT thin films on surface micromachined FPW devices with reasonable ferroelectric properties. Unfortunately, because of the deformation of the poly Si membranes and the low impedance due to the high dielectric constant these PZT film FPW devices were not able to be tested for acoustic response. The first SAW measurements for PZT thin film materials were obtained at frequencies on the order of 100 MHz. These were obtained for PNZT 2/52/48 films deposited on a nonconducting substrate ($LaAlO_3$). Attempts at using a ZrO_2 thin film // Si substrate underlying layer for a nonconducting substrate were not successful due to the surface roughness of the PZT thin film inhibiting interdigitated electrode definition. A number of process integration improvements for fabrication of PZT thin films on micromachined Si cantilever beams and SiN structures were developed. Both PZT//poly Si and PZT//low stress SiN cantilever beams were successfully fabricated. We also were able to develop a science based understanding of the change in piezoelectric response due to the formation of nanolayers on the underlying Ru electrodes of AlN films. Control of islands of RuO_2 at the interface of the AlN film is essential for reproducible piezoelectric response.

References

1. B.A. Tuttle, T.J. Headley, C. Drewien, J. Michael, J.A. Voigt and T.J. Garino, "Comparison of Ferroelectric Domain Assemblages in $Pb(Zr,Ti)O_3$ Thin Films and Bulk Ceramics," Ferroelectrics, (1998).
2. R.W. Schwartz, B.C. Bunker, D. Dimos, R.A. Assink, B.A. Tuttle, D.R. Tallant and I.A. Weinstock, "Solution Chemistry Effects in $Pb(Zr,Ti)O_3$ Thin Film Processing," Int. Ferroelectrics, vol.2, 243-54 (1992).
3. B.A. Tuttle and R.W. Schwartz, "Solution Deposition of Ferroelectric Thin Films," Mater. Res. Bulletin, Vol. 21 No.4, 36-46 (1996)
4. R.W. Schwartz, T.L. Recihert, P.G. Clem, D. Dimos and D. Liu, "A Comparison of Diol and Methanol-Based Chemical Solution Deposition Routes for PZT Thin Film Fabrication," Integrated Ferroelectrics, Vol. 18, pp. 275-86 (1997).
5. P.G. Clem, B.A. Tuttle, J.A. Voigt, T.J. Garino, and M. Rodriguez, " Design of CSD Routes for $BaTiO_3$, PZN/PT and PZT Thin Film Devices," The Tenth International Meeting of Integrated Ferroelectrics, Monterey, CA, March 1-4, 1998 (invited presentation).
6. W-C. Shih and M.-S.Wu, "Theoretical Investigation of the SAW Properties of Ferroelectric Film Composites," IEEE Trans on UFFC, vol. 45 [2] 305-16 (1998).6. T.J.,
7. S. J. Martin, M. A. Butler, J. J. Spates, M. A. Mitchell, and W. K. Schubert "Flexural plate wave resonator excited with Lorentz forces,", J. Appl. Phys., Vol 83, 4589 (1998).7.
8. T.J. Garino, P.G. Clem and B.A. Tuttle " The Fabrication of Piezoelectric Devices on Micromachined Si Beams," 9th Annual Symposium on Ceramics and Advanced Materials, Albuquerque, NM, Nov.3, 1997 .
9. B.A. Tuttle, T.J. Garino, P.G. Clem, D. Dimos, J.A. Ruffner, and W.K. Schubert, "Materials Analysis of $Pb(Zr,Ti)O_3$ Thin Film / Micromachined Si Structures," Fall 1997 Materials Research Society Meeting, Boston MA, 11/29 to 12/4/97 (invited presentation).

Distribution:

1	MS0188	D.L. Chavez. 04001
1	MS9018	Central Technical Files, 8940-2
2	MS0899	Technical Library, 4916
1	MS0619	Review & Approval Desk, 15102
1	MS0959	S.L. Lockwood, 01492
1	MS1080	J.H. Smith, 01725
1	MS1081	W.P. Eaton, 01728
1	MS1349	J.A. Ruffner, 01812
1	MS1349	T.J. Boyle, 01846
1	MS1349	T. Dunbar, 01812
5	MS1405	B.A. Tuttle, 01812
1	MS1405	W.R. Olson, 01812
1	MS1405	J.A. Voigt, 01846
1	MS1407	J.H. Aubert, 01815/12
1	MS1411	D. Dimos, 01831
1	MS1411	P. Clem, 01831
1	MS1411	T.J. Garino, 01846
3	MS1425	W.K. Schubert, 01715
1	MS1425	S.J. Martin, 01715
1	MS1425	M. Mitchell, 01715
1	MS1425	G. Frye, 01715
1	MS1425	J. Spates, 01715
1	MS1434	G.E. Pike, 01802